Available online at www.sciencedirect.com
ScienceDirect
Mathematical and Computer Modelling 47 (2008) 638–648
MATHEMATICAL AND COMPUTER MODELLING
www.elsevier.com/locate/mcm

Quantifying glioma cell growth and invasion *in vitro*

Kristin R. Swanson*

Laboratory of Neuropathology, Department of Pathology, Harborview Medical Center, Box 359791, Seattle, WA 98104-2499, USA
Department of Applied Mathematics, University of Washington, Box 352420, Seattle, WA 98105-2420, USA

Received 30 August 2006; accepted 20 February 2007

Abstract

A mathematical model has been developed to describe and quantify the growth and invasion of gliomas (the most common type of primary brain tumors). The model has already been shown to agree well with *in vivo* imaging studies of gliomas. Here we demonstrate the model's agreement with *in vitro* experimental data. The analysis provided in this article demonstrates that the model agrees well with published observations of growth and invasion of gliomas cells in culture. These *in vitro* results support the model's utility in describing the behavior of glioma cells in experimental settings but also lends credence to the applications of the model to the *in vivo* setting.

Keywords: Brain tumor; Mathematical model; Glioma; Invasion

1. Introduction

Gliomas are aggressive brain tumors with the ability to invade the surrounding normal tissue. Despite significant medical advances and concerted efforts to treat these tumors, the survival time for patients diagnosed with malignant gliomas remains a dismal 6–12 months [1]. To better characterize the behavior of gliomas, we have developed mathematical models for the growth and invasion of these brain tumors [2–4] under a variety of conditions ranging from *in vitro* experiments to actual *in vivo* dynamics. Our hope is that better treatment strategies can be found by studying virtual tumors via mathematical modeling. Mathematical models have been used extensively in the analysis of many biological phenomena (reviewed by [5]).

In vitro experiments are often used to analyze various aspects of *in vivo* behavior of biological systems. Since relevant *in vitro* experiments are often easier to perform, it is important to be able to interpret their results in qualitative and quantitative terms relevant to characterization of *in vivo* behavior. This modeling approach is used here to consider two such *in vitro* experiments [6,7] to better characterize and quantify glioma growth and invasion.

Gliomas originate from the structural cells of the central nervous system known as glial cells. Normal healthy glial cells have a very low motility rate [8] but malignant glial cells, glioma cells, have been shown to exhibit high motility

* Corresponding address: Laboratory of Neuropathology, Department of Pathology, Harborview Medical Center, Box 359791, Seattle, WA 98104-2499, USA.
E-mail address: swanson@amath.washington.edu.
URL: http://www.amath.washington.edu/~swanson.

0895-7177/$ - see front matter
doi:10.1016/j.mcm.2007.02.024

rates [6–17]. In the early 1980's, *in vitro* studies by Westermark et al. [18] demonstrated the remarkable motility of human malignant glioma cells. Using time-lapse video microscopy and other techniques, Chicoine and Silbergeld [6,8] have recently quantified brain tumor cell motility and invasion capabilities *in vivo* and *in vitro*. Their results [6] suggest an average linear velocity of 12.5 μm/h for human glioma cells *in vitro* and a minimum linear velocity of 4.8 μm/h *in vivo*.

In addition to those mentioned here, there has been a number of other experiments to quantify glioma growth and invasion [15,6,17,7,9,16,12–14,18]. The results of two of those experiments are particularly quantitative and thereby convenient to translate into the terms expressed in our mathematical model. We analyze those two experiments here.

2. Mathematical model

The basic mathematical model [2–4,19–22] is based on proliferation and migration of glioma cells and can be described by the word equation:

$$\begin{aligned}\text{rate of change of cancerous cell density} &= \text{diffusion (random motility) of the cancerous cells}\\ &\quad + \text{net proliferation of the cancerous cells}\end{aligned}$$

or in mathematical terms as

$$\frac{\partial \bar{c}}{\partial \bar{t}} = \bar{\nabla} \cdot (D(\bar{\mathbf{x}})\bar{\nabla}\bar{c}) + \rho\bar{c} \tag{1}$$

where $\bar{c}(\bar{\mathbf{x}}, \bar{t})$ is the tumor cell density at location $\bar{\mathbf{x}} = (\bar{x}, \bar{y})$ and time $\bar{t}$, D is the tumor cell motility rate (diffusion coefficient), and ρ represents the net proliferation rate of the tumor cells. We assume an exponential growth pattern for these types of tumor cells. Although a saturating growth term (e.g. logistic growth) would be strictly more accurate, we have found that on the time scale of the experiments concerned, the linear proliferative term is sufficient.

The brain consists of two types of tissue, grey matter and white matter. Gliomas migrate more quickly in white matter then in grey matter (see [2,3] for more details). For this reason, our model encompasses a diffusion coefficient which is a function of the spatial variable $\bar{\mathbf{x}}$ to differentiate regions of grey and white matter. We take the diffusion coefficient D to be a scalar; thus, we do not include any anisotropy in the brain tissue.

We use this basic model framework to quantify the experimental *in vitro* results observed by Chicoine and Silbergeld [6] and Giese et al. [9].

3. Chicoine and Silbergeld [6]: Radial dish assay experiments

Chicoine and Silbergeld [6] developed a tumor cell motility assay known as the "radial dish assay". In summary, 2×10^4 cells are plated in a central disc 2 cm in diameter on a petri dish 8 cm in diameter. The cells are poisoned to prevent mitosis. This poisoning of the cells to hinder mitosis is not thought to alter their motility [6]. Daily microscopy of the dish gives the redistribution of the cell population. For each day, the distribution of cells is plotted in Fig. 1, which is extracted from [6].

In this experiment, the cells are not allowed to proliferate ($\rho = 0$) and there is no presumed heterogeneity in diffusion ($D(\bar{x}) = D$). Under these conditions, the dimensional model given in Eq. (1) becomes:

$$\frac{\partial \bar{c}}{\partial \bar{t}} = D\bar{\nabla}^2\bar{c} \tag{2}$$

with zero flux boundary conditions at the edge of the petri dish:

$$\bar{\nabla}\bar{c}(\bar{r}, \bar{t}) \cdot \bar{\mathbf{n}} = 0 \quad \text{for } \bar{r} = R_0. \tag{3}$$

Here, R_0 is the radius of the petri dish. In the radial dish assay described by Chicoine et al. [6], $R_0 = 4$ cm. Initially cells are uniformly distributed in a central circular area of radius R corresponding to the initial condition:

$$\bar{c}(\bar{r}, 0) = c_0 H(R - \bar{r}) \tag{4}$$

where $\bar{r} = \|\bar{x}\|$ and H is a Heaviside function taking on the value 1 for $\bar{r} < R$ and 0 otherwise. In the experiments of Chicoine and Silbergeld [6], $R = 1$ cm. Since mitosis is blocked, there is no growth and a total of $N = c_0\pi R^2$ cells are in the petri dish during the entire experiment.

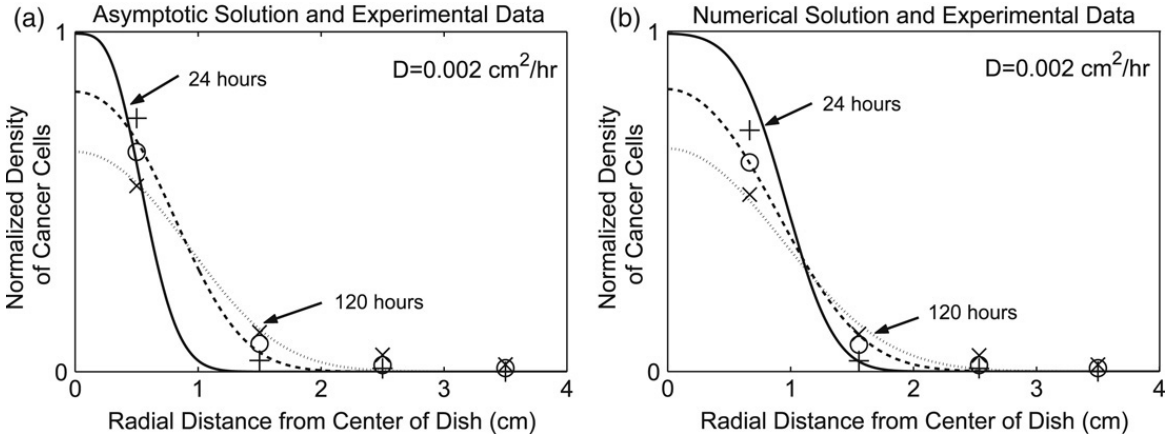

Fig. 1. Observations by Chicoine et al. [6] of *in vitro* cell densities compared with (a) asymptotic approximation (14) and (b) numerical solution of (3) and (4). The experimental data were extracted from Fig. 5 of Chicoine et al. [6] for mixed glioma cells. The asymptotic approximation shown in a) is strictly only valid for moderate t and small r (i.e. $\frac{r\lambda}{2t}$ small). The curves in (a) and (b) correspond to experimental observation times $t = 24$ (solid), 72 (dashed), 120 (dotted) h denoted by $+$, $\bigcirc$, $\times$, respectively. Parameter values: $D = 0.002$ cm^2/h, $\lambda = \frac{1}{4}$.

3.1. Nondimensionalization

Introducing the nondimensional variables:

$$\mathbf{x} = \frac{\bar{\mathbf{x}}}{R_0}, \qquad t = \frac{D}{R_0^2}\bar{t}, \qquad c(\mathbf{x}, t) = \frac{\bar{c}\left(\frac{\bar{\mathbf{x}}}{R_0}, \frac{D}{R_0^2}\bar{t}\right)}{c_0}, \tag{5}$$

where $N = c_0 \pi R^2$ represents the initial number of tumor cells in the brain at model time $t = 0$ and $\mathbf{x} = (x, y)$, the model in nondimensional terms becomes

$$\begin{aligned} &\frac{\partial c}{\partial t} = \nabla^2 c \quad \text{for } 0 < r < 1 \\ &c(r, 0) = H(\lambda - r) \\ &\nabla c \cdot \mathbf{n} = 0 \quad \text{at } r = 1, \end{aligned} \tag{6}$$

where $\lambda = \frac{R}{R_0}$. In the case of the radial dish assay experiments, $\lambda = \frac{1\text{ cm}}{4\text{ cm}}$. Equivalently, the nondimensional model can be written in radial coordinates as

$$\begin{aligned} &\frac{\partial c}{\partial t} = \frac{\partial^2 c}{\partial r^2} + \frac{1}{r}\frac{\partial c}{\partial r} + \frac{1}{r^2}\frac{\partial^2 c}{\partial \theta^2} \quad \text{for } 0 < r < 1 \\ &c(r, \theta, 0) = H(\lambda - r) \\ &\frac{\partial c}{\partial r} = 0 \quad \text{at } r = 1, \end{aligned} \tag{7}$$

where the tumor cell density c is now a function of radial distance $r = \sqrt{x^2 + y^2}$ and angle θ as well as time t.

3.1.1. Asymptotic approximation for cell density $c(r, \theta, t)$

Assuming that the petri dish is sufficiently large so that $R_0 \gg R$, the solution of (3) can be approximated by that on an infinite domain. This estimate is accurate as long as the cells are not motile enough to introduce significant boundary effects on the time scale of the experiment.

Solving Eq. (7) with a single delta function source of tumor cells at some location (η, σ) gives the fundamental solution

$$K(r, \theta, t; \eta, \sigma) = \frac{1}{4\pi t} \exp\left(-\frac{r^2 + \eta^2 - 2r\eta\cos(\theta - \sigma)}{4t}\right). \tag{8}$$

Since (7) is linear, superposition and the fundamental solution K to determine the solution of (7) with the experimental Heaviside initial conditions. If the initial area covered by tumor cells is small compared to the area of the entire petri dish, the distribution $c(r, \theta, t)$ can be approximated by the fundamental solution $K(r, \theta, t)$. However, in the case of the experiments of Chicoine and Silbergeld [6], the initial area covered by tumor cells is a significant fraction of the total area of the petri dish. Therefore, it is important to consider the short time effects of the initial condition (4).

First, consider the situation where the cells are initially distributed on an infinitesimally thin annulus (ring) of radius r_0:

$$c_{\text{ring}}(r, \theta, 0; r_0) = \frac{1}{2\pi r_0}\delta(r - r_0) = G(r, r_0). \tag{9}$$

By superposition, the solution of (3) with this annulus as the initial condition is

$$\begin{aligned} c_{\text{ring}}(r, \theta, t; r_0) &= \int_0^{2\pi}\int_0^{\infty} K(r, \theta, t; \eta, \sigma)G(r, r_0)\eta \mathrm{d}\eta \mathrm{d}\sigma \\ &= \frac{1}{8\pi^2 t}\int_0^{2\pi} \exp\left(-\frac{r^2 + r_0^2 - 2rr_0\cos(\theta - \sigma)}{4t}\right)\mathrm{d}\sigma \\ &= \frac{1}{8\pi^2 t}\exp\left(-\frac{r^2 + r_0^2}{4t}\right)\int_0^{2\pi}\exp(B\cos(\theta - \sigma))\mathrm{d}\sigma, \end{aligned} \tag{10}$$

where $B = \frac{rr_0}{2t}$. Note that this integral can be expressed as a modified Bessel function of order zero [24]:

$$c_{\text{ring}}(r, \theta, 0; r_0) = \frac{1}{4\pi t}\exp\left(-\frac{r^2 + r_0^2}{4t}\right) I_0\left(\frac{rr_0}{2t}\right). \tag{11}$$

Asymptotically, for small B,

$$\begin{aligned} \int_0^{2\pi}\exp(B\cos(\theta - \sigma))\mathrm{d}\sigma &= \int_{\theta - 2\pi}^{\theta}\exp(B\cos(z))\mathrm{d}z \\ &\sim 2\pi + \frac{\pi B^2}{2} + \frac{\pi B^4}{32} + O(B^6). \end{aligned} \tag{12}$$

For a ring of cells at a radius r_0 from the origin, the distribution of cells at some future time is given approximately by

$$c_{\text{ring}}(r, \theta, t; r_0) \sim \frac{1}{4\pi t}\exp\left(-\frac{r^2 + r_0^2}{4t}\right)\left(1 + \frac{B^2}{4} + O(B^4)\right) \quad \text{as } B \to 0. \tag{13}$$

When $B = 0$ (and thus $r_0 = 0$), this is the exact solution of (7) for a point source of cells at $r_0 = 0$.

To translate this result to the case of a disc of cells of radius R, recall that

$$\begin{aligned} c(r, \theta, 0) &= H(\lambda - r) \\ &= \int_0^{\lambda}\frac{\mathrm{d}}{\mathrm{d}r_0}(H(r_0 - r))\,\mathrm{d}r_0 \\ &= \int_0^{\lambda}\frac{\delta(r - r_0)}{2\pi r_0}2\pi r_0 \mathrm{d}r_0 \\ &= \int_0^{\lambda} c_{\text{ring}}(r, \theta, 0; r_0)2\pi r_0 \mathrm{d}r_0. \end{aligned}$$

Combining this with (13), the solution of the full problem (7) with disc initial conditions is

$$c(r,\theta,t) = \int_0^{\lambda} c_{\text{ring}}(r,\theta,t;r_0)2\pi r_0 \mathrm{d}r_0$$
$$\sim \exp\left(-\frac{r^2}{4t}\right)\left[\left(1-\exp\left(-\frac{\lambda^2}{4t}\right)\right)+\frac{r^2}{4t}\left(1-\exp\left(-\frac{\lambda^2}{4t}\right)\left(1+\frac{\lambda^2}{4t}\right)\right)\right]+\cdots \tag{14}$$

for $\nu = \frac{r\lambda}{2t}$ small. In the case of the experiments of Chicoine et al. [6], $\nu = \frac{r}{8t}$.

We use the approximate solution (14) to obtain an estimate for the diffusion coefficient for the glioma cells *in vitro*. Note that the estimate is expected to be most accurate for small r and/or $t = O(1)$ or larger. Fig. 1(a) is a plot of the experimental measurements of cell densities in the radial dish assay from Chicoine et al. [6] with the dimensional form of the asymptotic solution (14) for $D = 0.002\ \text{cm}^2/\text{h}$, the best fit of the model to the data, at the different experimental time points. The numerical solution of (3) and (4) for $D = 0.002\ \text{cm}^2/\text{h}$ with the experimental data from Fig. 1(a) is shown in Fig. 1(b). Comparison of Fig. 1(a) and (b) shows that the asymptotic approximation (14) is fairly accurate for determining an estimate of the diffusion coefficient parameter D.

3.2. Asymptotic approximation for $\langle r\rangle$

Chicoine et al. [6] also calculated the average distance from the origin, $\langle r\rangle$, for the glioma cells in the radial dish assay method. To determine $\langle r\rangle$ it is necessary to integrate the asymptotic solution (14) over all r values, but the asymptotic solution is strictly only valid for $\frac{r\lambda}{2t}$ small; this asymptotic parameter is not small for arbitrarily large r. Therefore, it is necessary to reconsider the approximation of $\langle r\rangle$.

Recall that if $c(r,\theta,t)$ is the distribution of the cells at time t, then the mean radial distance of cells from the origin $\langle r\rangle$ is given by

$$\langle r\rangle = \frac{\int_0^{2\pi}\int_0^{\infty} r c(r,\theta,t) r \mathrm{d}r\mathrm{d}\theta}{\int_0^{2\pi}\int_0^{\infty} c(r,\theta,t) r \mathrm{d}r\mathrm{d}\theta} = \int_0^{2\pi}\int_0^{\infty} c(r,\theta,t) r^2 \mathrm{d}r\mathrm{d}\theta \tag{15}$$

where

$$c(r,\theta,t) = \int_0^{2\pi}\int_0^{\infty} K(r,\theta,t;\eta,\sigma)H(\lambda-\eta)\eta\mathrm{d}\eta\mathrm{d}\sigma$$
$$= \int_0^{2\pi}\int_0^{\lambda} K(r,\theta,t;\eta,\sigma)\eta\mathrm{d}\eta\mathrm{d}\sigma \tag{16}$$

with K given by (8), then

$$\langle r\rangle = \int_0^{2\pi}\int_0^{2\pi}\left[\int_0^{\lambda}\eta\exp\left(-\frac{\eta^2}{4t}\right)\left[\int_0^{\infty} r^2\exp\left(-\frac{r^2-2r\eta\cos(\theta-\sigma)}{4t}\right)\mathrm{d}r\right]\mathrm{d}\eta\right]\mathrm{d}\theta\mathrm{d}\sigma$$
$$= \frac{1}{4\sqrt{\pi A}}\int_0^{2\pi}\int_0^{2\pi}\int_0^{\lambda}\eta^2(1+2A\cos^2(\theta-\sigma)\eta^2)$$
$$\times(1+\operatorname{erf}(\eta\sqrt{A}\cos(\theta-\sigma)))\exp(-A\eta^2\sin^2(\theta-\sigma))\mathrm{d}\eta\mathrm{d}\sigma\mathrm{d}\theta,$$

where $A = \frac{1}{4t}$. With the change of coordinates $u = \theta-\sigma$ and $v = \frac{1}{2}(\theta+\sigma)$, then

$$\langle r\rangle = \frac{2}{4\lambda^2\sqrt{\pi^3 A}}\int_0^{2\pi}\int_0^{\lambda}\eta(2\pi-u)(1+2A\eta^2\cos^2 u)(1+\operatorname{erf}(\eta\sqrt{A}\cos u))\exp(-A\eta^2\sin^2 u)\mathrm{d}\eta\mathrm{d}u.$$

For small t (large A), we use a Laplace's method argument to approximate this expression:

$$\langle r\rangle \sim \frac{3+2A\lambda^2}{6A\lambda}(1+\operatorname{erf}(\sqrt{A}\lambda)) - \frac{5}{6\lambda^2\sqrt{A^3\pi}} + \frac{5+2A\lambda^2}{6\sqrt{\pi}A\lambda^2}\exp(-A\lambda^2)$$
$$= \frac{6t+\lambda^2}{3\lambda}\left[1+\operatorname{erf}\left(\frac{\lambda}{2\sqrt{t}}\right)\right] - \frac{20}{3\lambda^2}\sqrt{\frac{t^3}{\pi}} + \frac{10t+\lambda^2}{3\sqrt{\pi}\lambda^2}\exp\left(-\frac{\lambda^2}{4t}\right)$$

$$\sim \frac{2\lambda}{3} + \frac{4t}{\lambda} + \cdots \quad \text{as } A = \frac{1}{4t} \to \infty. \tag{17}$$

As $t \to 0$ ($A \to \infty$), $\langle r \rangle$ approaches $\frac{2\lambda}{3}$ which corresponds to the exact mean radial distance associated with the (nondimensional) initial distribution of cells (4).

Alternatively, for large t (small A), the mean displacement can be expressed as

$$\langle r \rangle = \sqrt{\pi t}\left(1 + \frac{\lambda^2}{16t} - \frac{\lambda^4}{768t^2} + \cdots\right). \tag{18}$$

As expected, for t large, the mean radius converges to the case of a point source of cells at the origin: $\langle r \rangle = \sqrt{\pi t}$ (in dimensional form, $\langle \bar{r} \rangle = \sqrt{\pi D \bar{t}}$). That is, after an extended period of time, the diffusive forces will have spread the population out sufficiently so that the original distribution cannot be identified. However, for large time as well, the effects of the boundaries of the petri dish become important. In particular, since the cells in the petri dish are not allowed to grow during the experiments of Chicoine et al. [6], the cell density approaches a uniform steady state $c \to \lambda^2$ (in dimensional terms, $\bar{c} \to c_0\lambda^2$) as $t \to \infty$. Thus, a more accurate asymptotic estimate for the large time behavior would use this steady state to compute the mean displacement:

$$\langle r \rangle = \int_0^{2\pi}\int_0^{\infty} c(r,\theta,t) r^2 \mathrm{d}r\mathrm{d}\theta \to \int_0^{2\pi}\int_0^{1} \lambda^2 r^2 \mathrm{d}r\mathrm{d}\theta = \frac{2\pi}{3}\lambda^2 \quad \text{as } t \to \infty. \tag{19}$$

In Fig. 2, the small t and large t asymptotic approximations (17) and (18), the large time limit (19), and the numerical calculation of $\langle r \rangle$ for a given diffusion coefficient $D = 0.002$ cm^2/h are shown. For small t, the cells in the centrally located tumor cells are moving around within the initial core and have not yet meandered far from the edge of the original distribution. Therefore, the mean radius is slowly increasing linearly in time (17). Over time the cell spreading smears out the cell population and the original state of the cell distribution cannot be identified. The population approaches the behavior observed due to a point source of cells at the center of the petri dish (18). However, on comparison with the calculation of $\langle r \rangle$ from the numerical solution of (3) and (4), the asymptotic expansion for large t (18) becomes less valid due to the effects of the boundary (not incorporated into the approximation of $\langle r \rangle$). Those boundary effects are incorporated into the large time limit of $\langle r \rangle$ given in (19) and plotted in Fig. 2. For the range of diffusion coefficients that are biologically reasonable and that we therefore expect to observe (i.e. $D \approx 0.002$ cm^2/h), the asymptotic value $A = \frac{1}{4t}$ is large on the time scale of the experiments of Chicoine et al. [6]. That is, in dimensional terms, $A = \frac{R_0^2}{4D}(\bar{t})^{-1}$, where $\bar{t}$ lies between 0 and 168 h. For $D = 0.002$ cm^2/h, A lies between 11 and ∞ during these experiments. Fig. 2(b) demonstrates the small t (large A) asymptotic expansion is clearly more accurate than the large t (small A) expansion for the time scale of the experiments of Chicoine et al. [6].

Chicoine et al. [6] actually calculated a "mean radius" that is slightly different from what we calculated and described above for $\langle r \rangle$. Their calculation neglected the contribution of the cells within the initial ring of radius R. This corresponds to simply replacing the integral $\int_0^{\infty} \mathrm{d}r$ in the calculation of $\langle r \rangle$ (15) with the integral $\int_{\lambda}^{\infty} \mathrm{d}r$. We denote this new "mean radius" by $\langle r^* \rangle$. It satisfies:

$$\langle r^* \rangle = \frac{\int_0^{2\pi}\int_{\lambda}^{\infty}(r-\lambda)c(r,\theta,t)r\mathrm{d}r\mathrm{d}\theta}{\int_0^{2\pi}\int_{\lambda}^{\infty} c(r,\theta,t)r\mathrm{d}r\mathrm{d}\theta} = \frac{1}{1-\lambda^2}\int_0^{2\pi}\int_{\lambda}^{\infty}(r-\lambda)c(r,\theta,t)r\mathrm{d}r\mathrm{d}\theta, \tag{20}$$

where $c(r,\theta,t)$ is as previously defined in Eq. (16). Approximation methods similar to those above for $\langle r \rangle$ yield the following asymptotic approximation:

$$\langle r^* \rangle \sim \frac{2\pi t^2}{1-\lambda^2} + \frac{40}{3(1-\lambda^2)}\sqrt{\pi t^3} + \cdots \quad \text{for small } t \text{ (large } A\text{)}. \tag{21}$$

In the Chicoine et al. [6] experiments, $R = 1$ cm and therefore $\lambda = \frac{1}{4}$.

Fig. 3 shows the mean radius $\langle r^* \rangle$ computed from the experimental observations of Chicoine et al. [6] with the asymptotic expression (21) which is valid only for small t. There are three progressively malignant types of gliomas listed: anaplastic astrocytoma, mixed glioma and glioblastoma multiforme. Fig. 3 suggests estimates of 0.0016 cm^2/h, 0.002 cm^2/h, and 0.003 cm^2/h for the diffusion coefficients for anaplastic astrocytoma, mixed glioma,

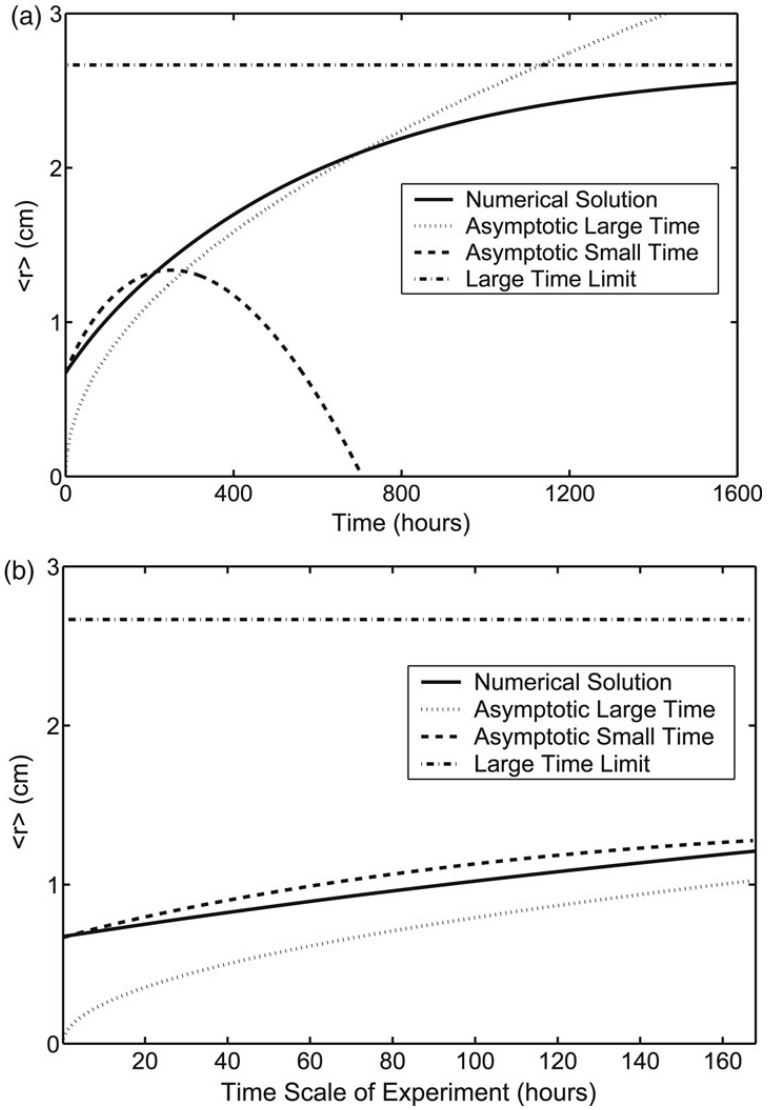

Fig. 2. (a) Numerical solution and asymptotic approximations of $\langle r \rangle$ for small and large t ((17) and (18)) as well as the large t limit (19) (b) Close up of figure (a) to show the portion of the time scale on which the experiments by Chicoine et al. [6] were observed. Parameter values: $D = 0.002\ \text{cm}^2/\text{h}$, $\lambda = \frac{1}{4}$.

and glioblastoma multiforme cells, respectively. Therefore, with increasing malignancy, cell motility appears to increase. In fact, this result suggests that there is approximately a two-fold difference between the motility of mid-grade anaplastic astrocytoma cells and high-grade glioblastoma cells.

In Fig. 3 the asymptotic expansion (17) overestimates the mean radius for glioblastoma cells for $\bar{t} > 96$ h [6]. This is expected because Chicoine et al. [6] observed that the glioblastoma cells move so quickly that they are capable of reaching the edge of the dish in 96 h [6], so that boundary effects become important. The anaplastic astrocytoma and mixed glioma cells are not capable of reaching the petri dish edge until later times.

As in the calculations of $\langle r \rangle$, there is a steady state limit that the tumor cell population in the petri dish is approaching ($c \to \lambda^2$) for large time. We can calculate the effect this steady state has on the limiting value of $\langle r^* \rangle$:

$$\langle r^* \rangle \to \frac{\int_0^{2\pi} \int_\lambda^1 (r - \lambda)\lambda^2 r \, dr \, d\theta}{\int_0^{2\pi} \int_\lambda^1 \lambda^2 r \, dr \, d\theta} = \frac{2 - 3\lambda + \lambda^3}{3(1 - \lambda^2)} \tag{22}$$

as $t \to \infty$. This limiting value of $\langle r^* \rangle$ is included in Fig. 3 as a dotted line. It defines the overestimation of $\langle r^* \rangle$ by the asymptotic approximation (17) for glioblastoma multiforme cells in Fig. 3(c).

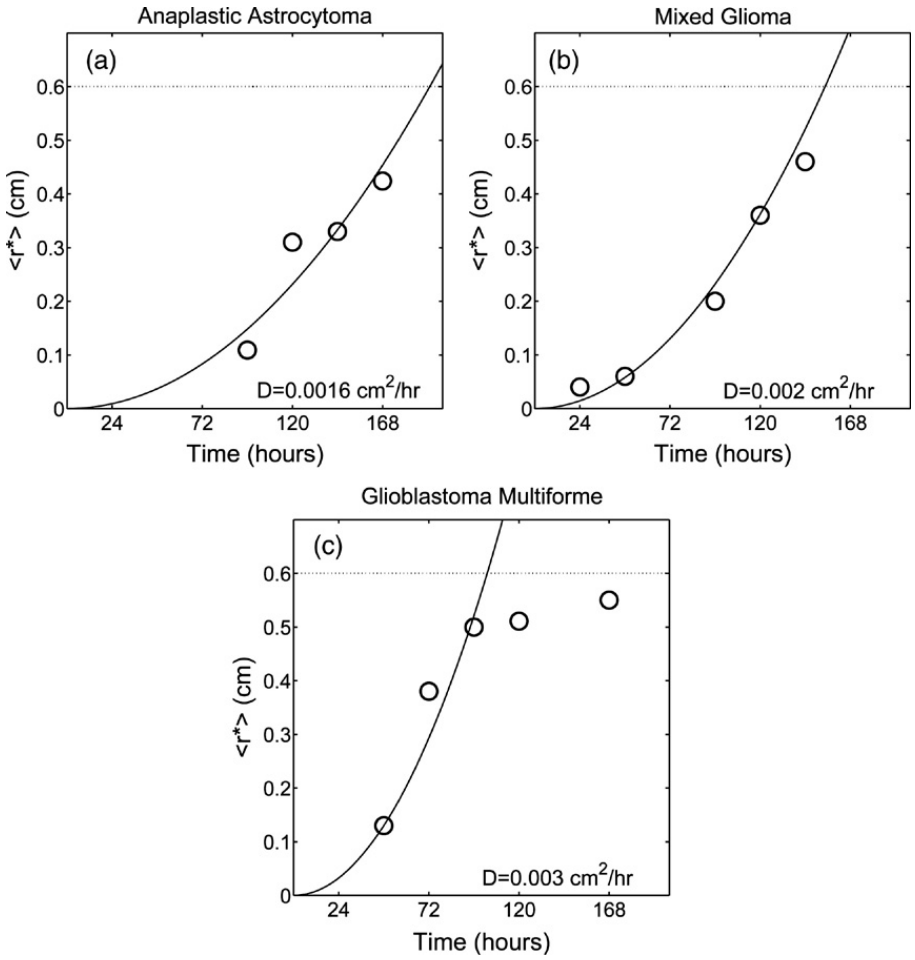

Fig. 3. Asymptotic approximation of mean radius $\langle r^* \rangle$ (21) versus time for a) anaplastic astrocytoma ($D = 0.0016$ cm^2/h), (b) mixed glioma ($D = 0.002$ cm^2/h) and (c) glioblastoma multiforme ($D = 0.003$ cm^2/h) cells (from Chicoine et al. [6]) where estimates of the diffusion coefficients were obtained by curve fitting. The uniform steady state solution defines the long time limit (dotted line) of $\langle r^* \rangle$ (22). The glioblastoma cells are observed to reach the edge of the petri dish by 96 h thus defining the overestimation of the asymptotic result for large t values in (c).

Chicoine et al. [23] used a modification of this radial dish assay to assess the chemo-attractant/repellent effects of certain cytokines on human glioma cell locomotion. An extension of the present modeling approach incorporating these experiments is in preparation.

4. Giese et al. [9]: Myelin motility experiments

Giese et al. [9] have characterized the increased motility of glioma cells in white matter by analyzing the motility of glioma cells on myelin (a key component of white matter) under experimental conditions. The experiments of Giese et al. [9] demonstrating that the motility of glioma cells is higher in white matter than that in the grey matter were similar to those of Chicoine et al. [6] but on a shorter time scale (40–100 h). The main difference between the two sets of experiments is that Giese et al. [9] allowed the cells to proliferate during the experiment. Giese et al. [9] tabulated the increase in radius of the visible front of tumor cells. Since the initially plated cells covered a smaller region than in the experiments of Chicoine et al. [6], the experiment should be modeled by Eq. (1) within the petri dish $\bar{r} \leq R_0$, where R_0 is the radius of the dish in which the cells are allowed to migrate and $\bar{r}^2 = \bar{x}^2 + \bar{y}^2$. This equation should be solved subject to zero flux boundary conditions

$$\bar{\nabla} \bar{c}(\bar{r}, \bar{t}) \cdot \mathbf{n} = 0 \quad \text{for } \bar{r} = R_0 \tag{23}$$

where $\mathbf{n}$ is the outward pointing normal at the edge of dish. Initially, there is a point source of N cells at the origin:

$$\bar{c}(\bar{r}, 0) = N\delta(\bar{r}). \tag{24}$$

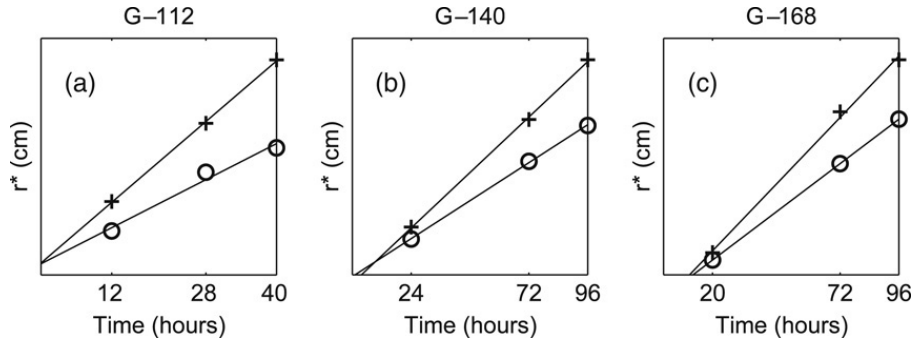

Fig. 4. Fit of model defined linear relationship between detectable radius r^* and time with experimental observations of Giese et al. [9] for three different glioblastoma cell lines: (a) G-112, b) G-140, (c) G-168 on the control substrate (ECM — extracellular matrix) (o) and white matter myelin (+). Slopes of each line define the velocity of the expanding tumor cell population and are shown in Table 1.

For sufficiently large R_0,

$$\bar{c}(\bar{r},\bar{t}) \sim \frac{N}{4\pi D\bar{t}} \exp\left(-\frac{\bar{r}^2}{4D\bar{t}}\right). \tag{25}$$

Giese et al. [9] determined the range of expansion of the population over time on myelin as compared to a control on ECM. That is, given some threshold of detection $\bar{c}^*$, the radius of the detectable tumor cell region was recorded as a function of time. The detectable radius $\bar{r}^*$ of the tumor cell population satisfies

$$\frac{\bar{r}^*}{\bar{t}} \sim 2\sqrt{D\rho} \tag{26}$$

for large $\bar{t}$. In other words, the velocity of the advancing detectable tumor cell region is approximately $2\sqrt{D\rho}$. Fig. 4 shows a linear least squares fit of the experimental observations of Giese et al. [9] of the detectable radius versus time for three glioblastoma cell lines (G-112, G-140, G-168) on myelin or ECM. The slope of each line is the velocity and is taken to be equal to $2\sqrt{D\rho}$. From an estimate of the growth rate ρ a diffusion coefficient D can be deduced from these linear-least-squares fits to the data. Table 1 gives the slopes of the linear fits shown in Fig. 4. Assuming that ρ is fixed whether the cells are migrating on the control extracellular matrix material (ECM) or on the myelin allows use of the slopes in Table 1 to deduce a relationship between the diffusion coefficients on ECM and myelin, as follows: Associate D_{ECM} and v_{ECM} to the diffusion coefficient and linear velocity of cells on ECM, respectively. Similarly, associate D_m and v_m to the diffusion coefficient and linear velocity of cells on myelin, respectively. The linear velocities satisfy

$$v_{\mathrm{ECM}} = 2\sqrt{\rho D_{\mathrm{ECM}}} \quad \text{and} \quad v_m = 2\sqrt{\rho D_m}. \tag{27}$$

Now the ratio of the diffusion coefficient on myelin to that on ECM is given by

$$\frac{D_m}{D_{\mathrm{ECM}}} = \left(\frac{v_m}{v_{\mathrm{ECM}}}\right)^2. \tag{28}$$

From the velocity values defined in Table 1 allow the deduction that the diffusion coefficient on myelin is 2– 3- times that on ECM.

As with all experimental results, it is unclear whether the behavior observed in the petri dish is analogous to that *in vivo*. To deal with this, a range of experimental conditions is often considered. Table 2 tabulates the results of another series of experiments by Giese et al. [11]. Each row of Table 2 corresponds to slightly different experimental conditions as defined by the amount of the nutrient fetal calf serum supplied to the cells. With increasing concentrations of serum (Experiments $1 \rightarrow 4$), the growth rate of the tumor cells increases but the motility reaches a maximum and then decreases. Fisher's approximation allows the deduction of the diffusion coefficients (D_{ECM}) for the glioblastoma cells in these four experimental conditions, as shown in Table 2. The diffusion coefficient also increases to a maximum and decreases with excess serum.

Table 1
Velocities v of detectable tumor radius as defined by the slopes of the linear-least-squares fits to the results of Giese et al. [9] shown in Fig. 4

Cell line	Velocity on myelin (cm/h) v_m	Velocity on ECM (cm/h) v_{ECM}	Ratio of diffusion coefficients in myelin and ECM D_m/D_{ECM}
G-112	.0026	.0015	3.00
G-140	.0019	.0013	2.14
G-168	.0035	.0025	1.96

Eq. (28) suggests there is a 2–3-fold difference between the diffusion coefficients on ECM and myelin under their experimental conditions.

Table 2
Experimental observations of Giese et al. [11] of the velocity of detectable tumor radius (v_{ECM}) in ECM and the growth rate (ρ)

Experiment number	Velocity on ECM v_{ECM} (cm/h)	Growth rate ρ (1/day)	Diffusion coefficient D_{ECM} (cm^2/h)
1	.0006	.075	.00003
2	.0012	.1	.00009
3	.00155	.2	.00007
4	.00115	.575	.00001

From v_{ECM} and ρ, the diffusion coefficient is deduced using the Fisher approximation (deducible from the model). Each row corresponds to different experimental conditions defined by the amount of fetal calf serum supplied to the cells.

5. Discussion

Gliomas are complicated to study and predict because their apparent growth as a mass consists of both proliferative expansion as well as motility of individual cells. The benefit of mechanistic modeling, like that presented in this manuscript, of *in vitro* brain tumor growth and invasion is that it provides a common language for the description of these observations. Since essentially every researcher has a different means of quantifying invasion versus proliferation, developing deterministic models like the one described here can assist researchers in the task of teasing out the contribution of both motility and proliferation in the overall dynamics of the tumor.

The present mathematical model for brain tumor cell growth and invasion *in vivo* and *in vitro* is based on net proliferation and cellular motility as the key elements of glioma behavior. The mathematical results compare well with the behavior observed experimentally by Chicoine et al. [6] and Giese et al. [9] as shown by the estimates of the parameters describing the two key components of glioma behavior: proliferation and invasion.

The strong agreement between experimental observations and the model predicted distribution suggests that the model sufficiently describes the key dynamics of gliomas *in vitro*. These results provide a foundation for using this model or a similar one for more complicated scenarios *in vivo*, as in a virtual three dimensional human brain matrix of grey and white matter [2,3]. This suggests that although it is a more complicated process to simulate tumor growth in virtual patients, the basic model mechanism may be the same for both *in vivo* and the simpler *in vitro* cases. In this article we have demonstrated that two different sets of experiments still retain the dynamics associated with our mathematical model components: proliferation and diffusive random motility.

The results of the comparison of our basic model results with *in vivo* studies has established a foundation for the development of our model for *in vivo* tumor growth and invasion. Although *in vivo* conditions are obviously different from *in vitro*, these experiments and the subsequent comparison with our model led us to a better understanding of glioma cellular behavior since it provides a means for quantification of experimental observations.

References

[1] J.M Nazzaro, E.A. Neuwelt, The role of surgery in the management of supranterorial intermediate and high-grade astrocyomas in adults, Journal of Neurosurgery 73 (1990) 331–344.
[2] K.R. Swanson, Mathematical modeling of the growth and control of tumors, Ph.D. Thesis, University of Washington, 1999.
[3] K.R. Swanson, E.C. Alvord Jr., J.D. Murray, A quantitative model for differential motility of gliomas in grey and white matter, Cell Proliferation 33 (2000) 317–329.
[4] K.R. Swanson, E.C. Alvord Jr., J.D. Murray, Virtual brain tumours (gliomas) enhance the reality of medical imaging and highlight inadequacies of current therapy, British Journal of Cancer 86 (2002) 14–18.

[5] J.D. Murray, Mathematical Biology, 3rd ed., Springer-Verlag, 2002.
[6] M.R. Chicoine, D.L. Silbergeld, Assessment of brain tumor cell motility *in vivo* and *in vitro*, Journal of Neurosurgery 82 (1995) 615–622.
[7] A. Giese, R. Schroder, A. Steiner, M. Westphal, Migration of human glioma cells in response to tumour cyst fluids, Acta Neurochirurgica 138 (1996) 1331–1340.
[8] D.L. Silbergeld, M.R. Chicoine, Isolation and characterization of human malignant glioma cells from histologically normal brain, Journal of Neurosurgery 86 (1997) 525–531.
[9] A. Giese, L. Kluwe, B. Laube, H. Meissner, M. Berens, M. Westphal, Migration of human glioma cells on myelin, Neurosurgery 38 (1996) 755–764.
[10] A. Giese, M. Westphal, Glioma invasion in the central nervous system, Neurosurgery 39 (1996) 235–252.
[11] A. Giese, M.A. Loo, N. Tran, D. Haskett, S.W. Coons, M.E. Berens, Dichotomy of astrocytoma migration and proliferation, International Journal of Cancer 67 (1996) 275–282.
[12] G.J. Pilkington, The paradox of neoplastic glial cell invasion of the brain and apparent metastatic failure, Anticancer Research 17 (1997) 4103–4106.
[13] G.J. Pilkington, *In vitro* and *in vivo* models for the study of brain tumor invasion, Anticancer Research 17 (1997) 4107–4110.
[14] J.H. Uhm, N.P. Dooly, J.G. Villemure, V.W. Yong, Mechanisms of glioma invasion: Role of matrix-metalloproteinases, Canadian Journal of Neurological Science 24 (1997) 3–15.
[15] V.R. Amberger, T. Hensel, N. Ogata, M.E. Schwab, Spreading and migration of human glioma and rat c6 cells on central nervous system myelin *in vitro* is correlated with tumor malignancy and involves a metalloproteolytic activity, Cancer Research 58 (1998) 149–158.
[16] T. Ohnishi, H. Matsumara, S. Izumoto, S. Hiraga, T. Hayakawa, A novel model of glioma cell invasion using organotypic brain slice culture, Cancer Research 58 (1998) 2935–2940.
[17] A. Giese, B. Laube, S. Zapf, U. Mangold, M. Westphal, Glioma cell adhesion and migration on human brain sections, Anticancer Research 18 (1998) 2435–2448.
[18] R. Westermark, A. Magnusson, C.H. Heldin, Effect of epidermal growth factors on membrane motility and cell locomotion in cultures of human clonal glioma cells, Journal of Neuroscience Research 8 (1982) 491–507.
[19] G.C. Cruywagen, D.E. Woodward, P. Tracqui, G.T. Bartoo, J.D. Murray, E.C. Alvord Jr., The modeling of diffusive tumours, Journal of Biological Systems 3 (1995) 937–945.
[20] D.E. Woodward, J. Cook, P. Tracqui, G.C. Cruywagen, J.D. Murray, E.C. Alvord Jr., A mathematical model of glioma growth: The effect of extent of surgical resection, Cell Proliferation 29 (1996) 269–288.
[21] P. Tracqui, G.C. Cruywagen, D.E. Woodward, G.T. Bartoo, J.D. Murray, E.C. Alvord Jr., A mathematical model of glioma growth: The effect of chemotherapy on spatio-temporal growth, Cell Proliferation 28 (1995) 17–31.
[22] P.K. Burgess, P.M. Kulesa, J.D. Murray, E.C. Alvord Jr., The interaction of growth rates and diffusion coefficients in a three-dimensional mathematical model of gliomas, Journal of Neuropathlogy and Experimental Neurology 56 (1997) 704–713.
[23] M.R. Chicoine, C.L. Madsen, D.L. Silbergeld, Modification of human glioma locomotion in vitro by cytokines EGF, BFGF, PDGFBB, NGF, and TNFα, Neurosurgery 36 (1995) 1165–1171.
[24] L. Råde, B. Westergren, Beta β Mathematics Handbook, 2nd ed., CRC Press, Boca Raton, 1990.